DOI: 10.1002/ejic.200901018

# Synthesis, Characterization and Combined Superoxide Dismutase and Catalase Activities of Manganese Complexes of 1,4-Bis(salicylidenamino)butan-2-ol

**Verónica Daier,[a] Diego Moreno,[a] Carine Duhayon,[b,c] Jean-Pierre Tuchagues,[b,c] and Sandra Signorella*[a]**

**Keywords:** Manganese / Superoxide dismutase / Catalase / Biomimetic catalyst / Kinetics / Enzyme catalysis

Two $Mn^{IV}$ complexes of general formula [Mn(salbutO)X] [$H_3$salbutO = 1,4-bis(salicylidenamino)butan-2-ol, **1**: X = $N_3$, **2**: X = SCN] have been prepared and structurally characterized. The crystal structure of **1** shows that salbutO$^{3-}$ acts as a pentadentate ligand through the two phenolato-*O*, two imino-*N*, and one alcoholato-*O* atoms, and the sixth coordination position is occupied by the azido-*N* atom, resulting in a slightly distorted $N_3O_3$ donor set around the $Mn^{IV}$ ion. ESI-MS, UV/Vis, and $^1$H NMR spectroscopy were used for solution studies. In methanol and dmf, the starting complexes are converted into [$Mn^{III}$(salbutO)] and its dimeric form. The $E_{1/2}$ of $Mn^{III}/Mn^{IV}$ (ca. 0.4 V vs. Ag/AgCl) allows this couple to efficiently catalyze the dismutation of $O_2^{\cdot-}$ with catalytic rate constant and $IC_{50}$ values of $1.91 \times 10^6$ $M^{-1}s^{-1}$ and 1.43 μM, respectively, which were obtained through the nitro blue tetrazolium photoreduction inhibition SOD assay, in aqueous solution of pH 7.8. The Mn-salbutO complexes also show catalase activity in methanol and dmf, with $k_{cat}$ = 1.6 $M^{-2}s^{-1}$ and 5.6 $M^{-1}s^{-1}$, respectively, an advantageous property for acting as scavenger of reactive oxygen species (ROS). This valuable conjunction of properties results from the conversion of [$Mn^{IV}$(salbutO)X] into [$Mn^{III}$(salbutO)]$_2$ in equilibrium with its monomer [$Mn^{III}$(salbutO)].

## Introduction

Manganese is known to be an essential element in many biological systems, and its oxidation-reduction chemistry is especially important for the electron-transfer reactions of mitochondrial superoxide dismutase, bacterial catalases, and photosystem II in green plant photosynthesis.[1] Catalases (CATs) and superoxide dismutases (SODs) efficiently catalyze disproportionation of intracellular $O_2^{2-}$ and $O_2^{\cdot-}$ and provide a vital biological defense against these toxic oxygen metabolites through a mechanism involving cyclic oxidation and reduction of the metal cofactor. In MnSODs, the active site contains one pentacoordinate Mn ion in a $N_3O_2$ environment,[2,3] whereas MnCATs catalyze the disproportionation of $H_2O_2$ by using a bis[μ-oxido(hydroxido)]-μ-carboxylatodimanganese structural unit as the active site.[4,5] Owing to their potential application as therapeutic agents against oxidative stress, various mononuclear Mn complexes have been selected for pharmaceutical uses as $O_2^{\cdot-}$ scavengers,[6–9] and a number of dinuclear manganese-based complexes has been investigated as low-molecular-weight catalytic scavengers of $H_2O_2$.[10–15] Particularly attractive are complexes exhibiting combined CAT and SOD activity, because they offer a possible therapeutic advantage arising from their multiple mechanism of action.[16–18] Here, we report the synthesis, structure, properties, and combined SOD and CAT activity of two novel manganese complexes, [Mn(salbutO)$N_3$] (**1**) and [Mn(salbutO)SCN] (**2**), based on the asymmetric Schiff base ligand 1,4-bis(salicylidenamino)butan-2-ol ($H_3$salbutO). Further, we compare their structure/activity with that of Mn complexes of symmetric Schiff base ligands with different aliphatic bridges, as a means to evaluate the effect of the length and symmetry of the aliphatic unit on the properties and activity of Mn complexes.

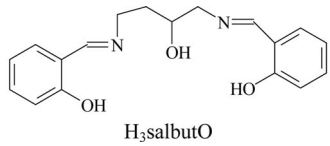


$H_3$salbutO

[a] IQUIR (Instituto de Química Rosario), CONICET, Universidad Nacional de Rosario
Suipacha 531, S2002LRK Rosario, Argentina
Fax: +54-341-4370477
E-mail: signorel@infovia.com.ar
[b] LCC (Laboratoire de Chimie de Coordination), CNRS
205, route de Narbonne, 31077 Toulouse, France
[c] UPS, INPT; LCC, Université de Toulouse
31077 Toulouse, France

Supporting information for this article is available on the WWW under http://dx.doi.org/10.1002/ejic.200901018.

## Results and Discussion

### Solid State Characterizations

#### *Crystal structure of [Mn(salbutO)($N_3$)] (1)*

The lattice consists of discrete Mn(salbutO)$N_3$ molecules. The molecular structure of complex **1** is illustrated in Fig-

 © 2010 Wiley-VCH Verlag GmbH & Co. KGaA, Weinheim 

ure 1, together with relevant bond lengths and angles. The asymmetric unit consists of crystallographically independent Mn complex molecules in which salbutO$^{3-}$ acts as a pentadentate ligand through the two phenolato-*O*, two imino-*N*, and one alcoholato-*O* atoms, and the sixth coordination position is occupied by the azido-*N* atom, resulting in a $N_3O_3$ donor set. The coordination environment around the Mn center can be described as slightly distorted octahedral. Most *cis* and *trans* angles at the metal center are in the range 88.54–92.28° and 177.53–178.24°, respectively. The O2–Mn1–O1, O2–Mn1–N2, and O2–Mn1–O3 angles differ by 4–8° from the ideal ones because of ligand constraints imposed by the adjacent five- and six-membered chelate rings. In this compound, the $Mn^{IV}$ cation accommodates the pentadentate ligand forming four adjacent six-six-five-six-membered chelate rings. The different bite angles and flexibilities of the methylene and ethylene bridges sustain the observed distortion of the coordination octahedron.

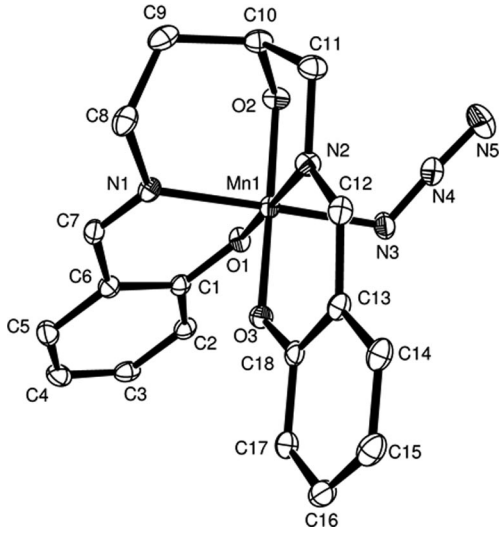


Figure 1. Plot of the asymmetric unit of [Mn(salbutO)$N_3$] (**1**) at the 30% probability level with atom numbering. Hydrogen atoms have been omitted for clarity. Selected bond lengths (Å) and angles (°): Mn1–N1 2.008(2), Mn1–N2 1.983(2), Mn1–N3 1.991(2), Mn1–O1 1.8619(17), Mn1–O2 1.8482(18), Mn1–O3 1.8926(18), N1–Mn1–N3 178.24(10), N2–Mn1–O1 177.53(8), O3–Mn1–O2 171.94(8), N1–Mn1–N2 92.28(9), N3–Mn1–N2 89.43(10), N1–Mn1–O3 88.70(9), N3–Mn1–O3 90.85(9), N2–Mn1–O3 90.36(8), N1–Mn1–O1 88.87(8), N3–Mn1–O1 89.44(9), O3–Mn1–O1 91.86(8), N1–Mn1–O2 88.54(9), N3–Mn1–O2 92.1(1), N2–Mn1–O2 82.19(8), O1–Mn1–O2 95.65(8).

The average Mn–O/N distance of 1.931 in complex **1** compares well with those reported for another $Mn^{IV}O_3N_3$ Schiff base complex (Mn–O/$N_{av}$ 1.934 Å),[19] the Mn–$N_{azido}$ length of 1.991 Å in **1** is shorter than those found for $Mn^{III}$ complexes (2.21–2.35 Å),[20,21] and the Mn–$O_{phenoxo}$ and Mn–$N_{imino}$ distances in **1** lie within the respective ranges of 1.82–1.92 and 1.981–2.01 Å found for other structurally characterized $Mn^{IV}$ complexes of Schiff base ligands.[22–29] It is important to notice that, although there is a marked decrease in metal–ligand bond lengths when $Mn^{IV}$ Schiff base complexes are compared with those of $Mn^{II}$ (i.e. $Mn^{II}$–$O_{phenoxo}$ 2.054, $Mn^{II}$–$N_{imino}$ 2.258 Å),[30] there is little difference from metal–ligand bond lengths of $Mn^{III}$ Schiff base complexes ($Mn^{III}$–$O_{phenoxo}$ 1.855–1.902 and $Mn^{III}$–$N_{imino}$ 1.987–2.044 Å).[31–35] However, like most $Mn^{IV}$ complexes with octahedral coordination environment,[26,28,29,36] the pseudo-octahedral $O_3N_3Mn$ polyhedron in **1**, although showing a slight axial elongation along N1···N3 (average values of 2.000 and 1.896 Å for the axial and equatorial bonds, respectively), does not show the Jahn–Teller distortion typical of $Mn^{III}$.

The crystal packing of complex **1** (Figure 2) may be described as an extended 3D network due to numerous intermolecular hydrogen-bonding contacts (20 for each complex molecule) involving the oxygen atoms from coordinated alkoxide and phenoxide groups, both terminally coordinated and uncoordinated azido nitrogen atoms, and imino, phenolic, and aliphatic carbon atoms. A more detailed description is of interest: As shown in Figure 2, the unit cell ($z$ = 4) includes four symmetry-related molecules, where the basic one (A, $x$, $y$, $z$) and its congener through the inversion center (D, 1–$x$, 1 – $y$, 1 – $z$) are connected to molecules C (1/2 + $x$, 1/2 – $y$, –1/2 + $z$) and B (1/2 – $x$, 1/2 + $y$, 1.5 – $z$), respectively, through four contacts (C11H···O1 3.248, C12H···O2 3.176, C14H···O2 3.302, and C14H···C10, 3.588 Å). These two pairs of complex molecules are interconnected through C5H···N5 (A···C) and N5···HC5 (B···D), 3.497 Å, contacts. In addition, each complex molecule of the unit cell is connected to seven molecules of adjacent units. As an example, for A, the contacts involved are {C3H···N3 and N3···HC3}, 3.265 Å (E, –$x$, –$y$, 1 – $z$), N5···HC5 (G, –1/2 + $x$, 1/2 – $y$, 1/2 + $z$), N5···HC16 (I, 1/2 + $x$, 1/2 – $y$, 1/2 + $z$), C16H···N5 (J, –1/2 + $x$, 1/2 – $y$, –1/2 + $z$), {C15···HC8 3.467, C16···HC8 3.593, C17···HC8 3.814 Å} (F, –1 + $x$, $y$, $z$), {C8H···C15, C8H···C16, C8H···C17} (K, 1 + $x$, $y$, $z$), and {O1···HC11, O2···HC12,

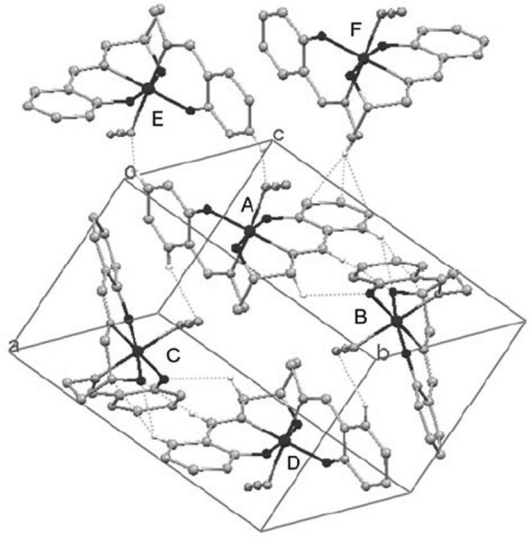


Figure 2. Crystal packing diagram for **1**, emphasizing the intermolecular hydrogen-bonding interactions.

 © 2010 Wiley-VCH Verlag GmbH & Co. KGaA, Weinheim 

O2···HC14, C10···HC14} (L, 1/2 – $x$, –1/2 + $y$, 1.5 – $z$). As a result, the supramolecular network is made of complex molecules of **1** tightly associated in one-dimensional (1D) chains through the C11H···O1, C12H···O2, C14H···O2, and C14H···C10 contacts; these chains are in turn more loosely interconnected to yield a 3D network through the C3H···N3, C5H···N5, C16H···N5, C8H···C15, C8H···C16, and C8H···C17 contacts described above (Table S1).

### *Magnetic Properties*

The room-temperature magnetic moment ($\mu_{eff}$) of complexes **1** and **2** in the solid state is 4.04 and 4.09 BM, respectively, close to the spin-only magnetic moment expected for a $d^3$ ion ($\mu_{SO}$ = 3.87 MB for $g$ = 2). Variable-temperature magnetic susceptibility measurements on **1** and **2** were performed in the 2 to 300 K temperature range on cylindrical pellets of 3 mm diameter pressed from ground microcrystals. Plots of the inverse corrected molar susceptibility vs. temperature yielded straight lines, indicating Curie–Weiss behavior. The temperature intercept of these plots gave experimental Weiss constants ($\theta$) of –1.84 K for **1** and –6.6 K for **2**. The Curie constant ($C$) values of 2.05 (**1**) and 2.2 (**2**) are also close to the expected value for one non-interacting $Mn^{IV}$ ion ($S$ = 3/2 and $g$ = 2), and the negative $\theta$ value suggests the operation of weak antiferromagnetic interactions in these complexes. Considering the mononuclear nature of **1** and **2** and the molecular structure of **1**, their magnetic behavior may originate from antiferromagnetic intermolecular spin–spin interactions and/or single-ion zero-field-splitting (zfs) of $Mn^{IV}$, the latter effect being usually weak in the case of $Mn^{IV}$. In view of the minute axial elongation of the coordination octahedron along N1···N3 in **1**, we neglected the possible operation of axial zfs. Taking into account the 1D chains formed through C11H···O1, C12H···O2, C14H···O2, and C14H···C10 contacts, we fitted the magnetic data by considering chain interactions. As shown in Figure S1 and Figure 3 for **1** and **2**, respectively, the fits obtained when computing the magnetic susceptibility with the assumption of a Heisenberg chain of $S$ = 3/2 spins[37] were fairly good for the parameter values $g$ = 2.065 (**1**), 2.04 (**2**); $J$ ($cm^{-1}$) = –0.05 (**1**), –0.30 (**2**); Par (paramagnetic contribution) = 0.6% (**1**), 0.05% (**2**), agreement factor $R = \Sigma[(\chi_M T)_{obs} - (\chi_M T)_{calc}]^2/\Sigma[(\chi_M T)_{obs}]^2$ = 4.7 $10^{-5}$ (**1**), 1.3 $10^{-4}$ (**2**).

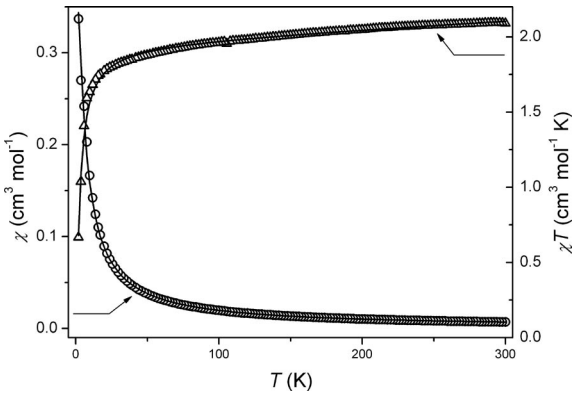


Figure 3. Temperature dependence of $\chi_M$ (○) and $\chi_M T$ (Δ) for compound **2**. The solid lines show the best fit based on the Heisenberg chain model (see text).

### *FTIR Spectroscopy*

Comparison of the IR spectra of **1** and **2** evidences the "fingerprint" pattern of salbut$O^{3-}$ coordinated to the Mn ion and confirms their analogous structures. The IR spectra of complexes **1** and **2** (Figure 4) exhibit strong imine and phenolato absorptions at 1618 and 1605 $cm^{-1}$, downshifted by approximately 15 $cm^{-1}$ from those in the free ligand because of the coordination of the metal to these groups, and one strong band at 2031 (**1**) [2058 (**2**)] $cm^{-1}$ attributable to coordinated $N_3^-$ [$SCN^-$], in agreement with their molecular structure. Powder samples of both compounds display a broad band at approximately 3450–3400 $cm^{-1}$ assigned to non-coordinated water molecules. Except for the $\nu_{OH}$ absorption, the powder and crystalline samples of **1** show identical IR spectra.

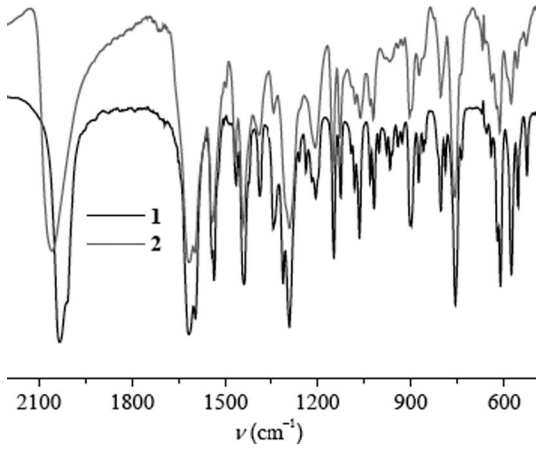


Figure 4. FTIR spectra of complexes **1** and 2.

## Solution Studies

### *UV/Vis Spectra*

The UV/Vis spectrum taken immediately after preparing a dmf solution of complex **1** [Figure 5(a)] is characterized by three absorption bands at 340 nm (8680 $M^{-1}cm^{-1}$), 400 nm (6730 $M^{-1}cm^{-1}$), and 490 nm (4000 $M^{-1}cm^{-1}$). The electronic spectrum of this complex is in agreement with those reported for other mononuclear $Mn^{IV}$ Schiff base complexes.[26,28] The strong absorbance at 340 nm can be assigned to a ligand-centered transition, while the other two intense absorptions of lower energy are likely to be phenolato-to-$Mn^{IV}$ charge-transfer transitions, as observed for other $Mn^{IV}$ complexes with phenoxido ligands.[22–24,26] These strong charge-transfer transitions probably obscure the low-intensity ($\varepsilon \leq 200\ M^{-1}cm^{-1}$) absorption bands expected for the $Mn^{IV}$ $^4A_{2g} \rightarrow {}^4T_{2g}$ and $^4A_{2g} \rightarrow {}^4T_{1g}$ d–d transitions (octahedral approximation).

 © 2010 Wiley-VCH Verlag GmbH & Co. KGaA, Weinheim 

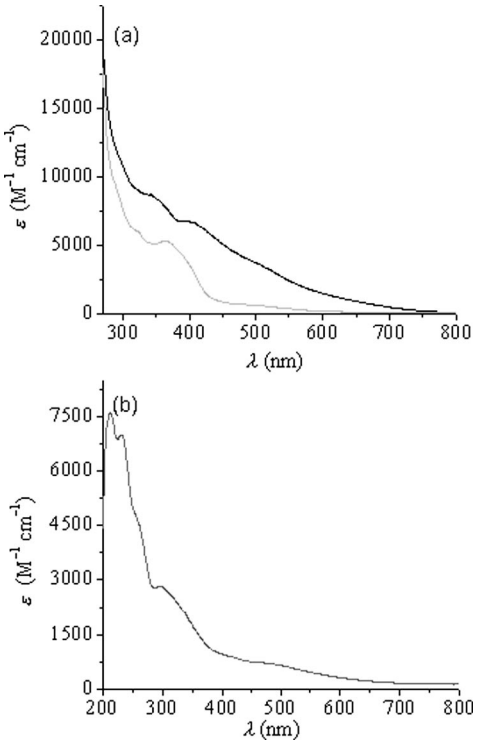


Figure 5. Electronic spectra of **1** (a) immediately (black line) and 30 min (gray line) after dissolution in dmf; (b) in methanol.

The initial spectrum of a $5 \times 10^{-5}$ M solution of **1** in dmf gradually changed to the gray line spectrum shown in Figure 5(a) as time passed. After 30 min, the spectrum did not exhibit any further change. The spectrum of the new species formed in solution is characterized by three absorption bands at 315 nm (6300 $M^{-1}cm^{-1}$), 365 nm (5300 $M^{-1}cm^{-1}$), and 500 nm (645 $M^{-1}cm^{-1}$), which can be assigned to intraligand π–π*, phenolato→M charge-transfer, and d–d transitions, respectively. The energy and intensity of the LMCT and d–d transitions are in agreement with those reported for related $Mn^{III}$ complexes.[32,33,38] These results indicate that the $Mn^{IV}$(salbutO)$N_3$ complex is not stable in solution and converts to a $Mn^{III}$ complex. The stability of the $Mn^{IV}$ complex in solution is significantly decreased by the presence of trace HCl or increased amounts of $H_2O$ in the solvent. More concentrated dmf solutions of **1** require longer times for complete conversion to the reduced $Mn^{III}$ form. Water substitution of the azide anion followed by oxidation of coordinated water could be responsible for the $Mn^{IV}$ redox instability in solution. The lower water to complex ratio in the more concentrated solutions of **1** would explain the slower reduction. Alternatively, the redox instability of **1** could be due to the presence of trace amounts of methanol or dimethylamine, which are difficult to avoid in dmf.

Diluted $5 \times 10^{-5}$ M solutions of **2** in dmf rapidly convert to the $Mn^{III}$ species, and the first electronic spectrum taken after mixing corresponds to the $Mn^{III}$ complex, thus indicating the lower stabilizing effect of $SCN^-$ vs. $N_3^-$.

The electronic spectra of solutions of complexes **1** and **2** in methanol showed immediate conversion to the corresponding $Mn^{III}$ complex. In this solvent, the electronic spectrum [Figure 5(b)] is characterized by two strong absorptions at 215 nm (7590 $M^{-1}cm^{-1}$) and 233 nm (6980 $M^{-1}cm^{-1}$), corresponding to ligand-centered transitions: one phenolato-to-metal charge-transfer at 298 nm (2820 $M^{-1}cm^{-1}$) and a weak d–d transition at 480 nm (700 $M^{-1}cm^{-1}$) with the characteristic intensity of $Mn^{III}$ complexes.[32,33,38] The protic solvent probably facilitates the loss of the coordinated azide anion (as observed in the ESI mass spectra) resulting in the decrease of the redox stability of the $Mn^{IV}$ complex that converts to the $Mn^{III}$ species.

### *ESI Mass Spectrometry (ESI-MS)*

ESI mass spectra of complexes **1** and **2** in methanol or acetonitrile confirmed their chemical composition in solution. For both complexes, the main peak is observed at *m*/*z* = 365 (100% intensity) in the positive mode ESI mass spectra [see Figure 6(a) for the spectrum of **2**] and originates from the $[Mn(salbutOH)]^+$ monocation. In the whole set of mass spectra registered at different times and complex concentrations, two other peaks are observed at *m*/*z* = 728 and 729, the isotopic pattern of which matches very well the simulated spectra for dimers $[Mn_2(salbutO)_2]^+$ and $[Mn_2(salbutO)_2H]^+$ (Figure S2). Since the $Mn^{III}Mn^{IV}$ mixed-valence species $[Mn_2(salbutO)_2]^+$ is not observed by EPR spectroscopy, it must be generated within the spectrometer from the neutral $[Mn_2(salbutO)_2]$ dimer. The coexistence of neutral and cationic $[Mn^{III}(salbutO(H))]^{0/+}$ and $[Mn^{III}_2(salbutO(H))_2]^{0/+}$ species in solution could be the cause of the low molar conductivity value measured for these compounds in methanol. The intensity of the peaks at *m*/*z* = 728 (729) relative to the monomer (*m*/*z* = 365) decreases from acetonitrile to methanol [Figure 6(a) and Figure S3]. Moreover, addition of $HClO_4$ (1 μM) to the methanol solution of the complex causes further decrease in the intensity of the peak at *m*/*z* = 728 to around 5% of

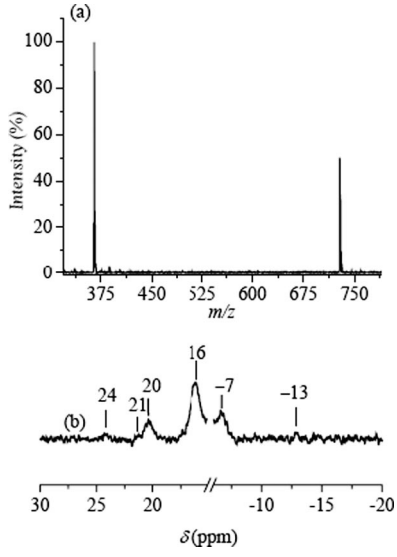


Figure 6. ESI mass spectrum of **2** in acetonitrile (a) and $^1H$ NMR spectrum of **2** in [$D_4$]methanol (ca. 10 mM) (b).

 © 2010 Wiley-VCH Verlag GmbH & Co. KGaA, Weinheim 

the main peak with $m/z$ = 365. The peaks belonging to the dimeric species disappear when $[HClO_4] \geq 0.10$ mM (Figure S4), thus showing that protons disfavor dimer formation.

### *$^1$H NMR Spectroscopy*

NMR spectroscopy has proved to be a useful probe of the ligand conformation for Schiff base complexes of Mn in solution. In Mn–salicylidenamino complexes, the resonances of the protons *ortho* to the *O*-phenoxide (H3) and imino (H6) groups of the ligand are normally too broad to be detected because of their closeness to the Mn center.[39] Therefore, $^1$H NMR spectra of tetragonal mononuclear Mn complexes with Schiff base ligands symmetrically positioned in the equatorial plane show two up-field resonances around –20 to –25 ppm assigned to H4 and H5 protons of the phenolato ring.[40–43] However, a more complex pattern is observed in the $^1$H NMR spectra of Mn complexes in which the ligand is not symmetrically positioned around the Mn ion.[31b,40] The paramagnetic $^1$H NMR spectra of complexes **1** and **2** in [$D_4$]methanol show a common pattern with five signals ranging from +24 to –13 ppm [Figure 6(b)]. Resonances observed at 24, 16, –7, and –13 ppm may arise from two pairs of nonequivalent H4, H5 ring protons, while the signals at 20 and 21 ppm may arise from the methylene protons of the butane backbone.[31b] The magnetic nonequivalence of the phenolato protons may be the result of the different extent of spin delocalization over the protons of the phenolato *trans* to the imine group vs. that of the phenolato *trans* to the alcoholato-*O* atom. Therefore, $^1$H NMR spectra indicate that the arrangement of the ligand in the solid state is retained in solution, in both the monomer and dimer forms of the complex.

### *Electrochemical Studies*

The electrochemical properties of complexes **1** and **2** were investigated by cyclic, linear, and square-wave voltammetry in methanol and dmf solutions containing 0.1 M $Bu_4NPF_6$. In methanol, the two complexes show the same electrochemical behavior, in agreement with the analogous spectroscopic pattern they exhibit in this protic solvent. The cyclic voltammograms of **1** and **2**, taken 30 min after the preparation of their methanol solutions, display one quasi-reversible oxidation wave at $E_{1/2}$ = 425 mV, with a peak-to-peak separation of 110 mV (at 100 mV/s scan rate), slightly above the value expected for a one-electron electrochemically reversible process, and a nonreversible reduction at –450 mV [Figure 7(a)]. Voltammetry at a rotating electrode confirmed that the waves at 425 mV and –450 mV correspond to an oxidation and a reduction process, respectively. $W_{1/2}$ values of approximately 130 mV in the square-wave voltammetry experiments suggest that they correspond to one-electron processes attributed to the $Mn^{III}/Mn^{IV}$ and $Mn^{III}/Mn^{II}$ redox couples. The irreversibility of the reduction process suggests that reduction to $Mn^{II}$ results in a chemically transformed species generated at the electrode. The additional peak at 880 mV observed in the anodic scan corresponds to the oxidation of the $SCN^-$ anion.

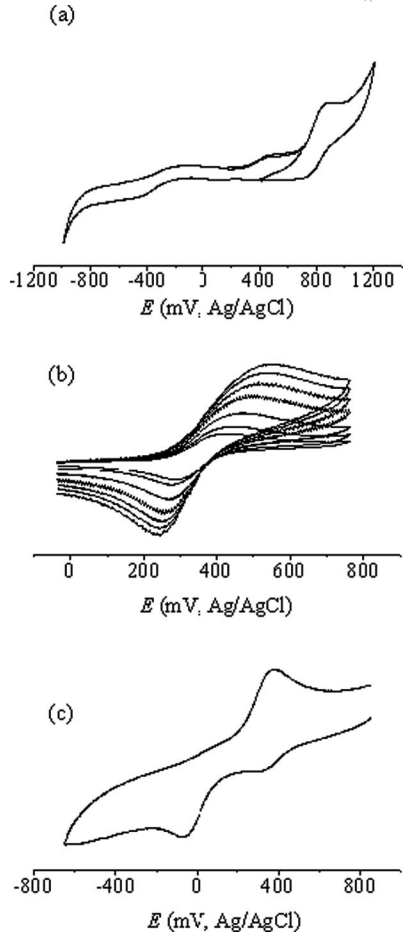


Figure 7. Cyclic voltammogram of (a) **2** in methanol, (b) **2** in dmf at various scan rates between 50 and 1000 mV, and (c) **1** in dmf a few minutes after dissolution. Conditions: Pt/Pt/Ag/AgCl; conc.: 1 mM; supporting electrolyte: $Bu_4NPF_6$. Scan rate in (a) and (c): 100 mV $s^{-1}$.

Voltammograms of dmf solutions of complex **2** recorded at different times show a quasi-reversible oxidation wave at 360 mV that corresponds to the $Mn^{III}/Mn^{IV}$ couple, as confirmed by linear and square-wave voltammetry. This process is diffusion-controlled. Cyclic voltammograms at different scan rates are shown in Figure 7(b). An additional nonreversible reduction wave that corresponds to the $Mn^{III}/Mn^{II}$ couple was observed at around –400 mV in the cathodic scan. In addition, the voltammogram displays one additional peak in the anodic scan at $E_{1/2}$ = 1140 mV that corresponds to the oxidation of the $SCN^-$ anion.

In the voltammograms recorded immediately after preparation of dmf solutions of complex **1** [Figure 7 (c)], a nonreversible reduction peak was observed at –66 mV, in addition to the quasi-reversible oxidation wave at 360 mV corresponding to the $Mn^{III}/Mn^{IV}$ couple analogous to that observed in dmf solutions of complex **2**. The reduction peak may correspond to the $Mn^{IV}/Mn^{III}$ couple of the [$Mn^{IV}$(salbutO)$N_3$] complex **1**, while the oxidation wave may be attributed to the $Mn^{III}/Mn^{IV}$ couple of the [$Mn^{III}$(salbutO)] complex formed upon loss of the azido ligand. The assignment of the peak at –66 mV to the reduction of [$Mn^{IV}$-

 © 2010 Wiley-VCH Verlag GmbH & Co. KGaA, Weinheim 

(salbutO)$N_3$] is supported by the increased intensity of the oxidation peak of the free azide at $E_{1/2}$ = 1130 mV upon decrease in intensity of the peak at –66 mV.

The $Mn^{IV}/Mn^{III}$ redox potential of [Mn(salbutO)] is similar to those of $[Mn(salpn)(OMe)]_2$ [458 mV vs. Ag/AgCl, $H_2$salpn = 1,3-bis(salicylidenamino)propane] and [Mn(salpn)(acac)] (523 mV vs. Ag/AgCl), which have a *cis*-β-tetradentate salpn ligand,[31b] but much lower than those found for the tetragonal complexes $[Mn(salpn)(MeOH)_2]^+$ and $[Mn(salpnOH)]^+$ [$H_3$salpnO = 1,3-bis(salicylidenamino)-propan-2-ol],[40] with the ligand in the equatorial plane and no alkoxido group bound to Mn. The latter complexes show $Mn^{III}/Mn^{II}$ reduction at –98 and –172 mV vs. Ag/AgCl (methanol), respectively, without a metal-centered oxidation wave in the anodic scan. The redox potential of the $Mn^{III}/Mn^{IV}$ couple of [Mn(salbutO)] is also similar to that found for $[(Mn_2salpentO)(OMe)(OAc)]^+$ [384 mV vs. Ag/AgCl, $H_3$salpentO = 1,5-bis(salicylidenamino)pentan-3-ol],[44] in which the ligand is located in the meridional plane affording six-membered chelate rings around each manganese ion. In addition, salbut$O^{3-}$ stabilizes $Mn^{IV}$ complexes more poorly than other ligands with a similar donor set that form five-membered chelate rings around Mn.[26] Thus, the presence of the coordinated alkoxido group combined with the ligand arrangement around the metal center and the size of the chelate rings adjust the potential of the $Mn^{III}/Mn^{IV}$ cycle in [Mn(salbutO)] to approximately 400 mV.

### *SOD Activity*

In order to evaluate the activity of complexes **1** and **2** toward superoxide in aqueous buffer, the nitro blue tetrazolium (NBT) assay was used. This assay is based on kinetic competition for the superoxide reaction between NBT and the complex with SOD activity. In this way, the SOD activity is inversely related to the amount of formazan, the purple product formed by reaction of NBT with superoxide, observed at 560 nm. When added to the reaction mixture, both **1** and **2** were found to inhibit the reduction of NBT, as shown in Figure 8.

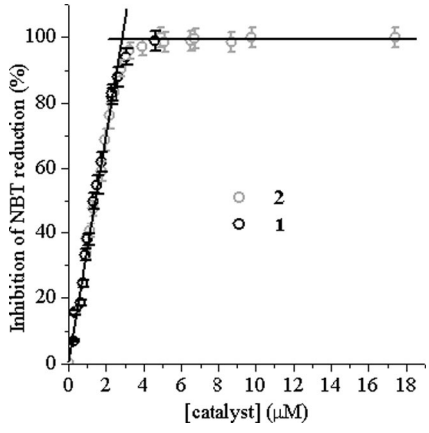


Figure 8. SOD activity of complexes **1** and **2** in the riboflavin-methionine-NBT assay.

Inhibition percentages were measured for several complex concentrations, and the $IC_{50}$ value, graphically evaluated, was 1.43 μM for the two complexes. On the basis of competition with NBT, at 50% inhibition, the rates of the reactions of NBT and the mimic with $O_2^{\cdot-}$ are equal, $k_{cat}$ [catalyst] = $k_{NBT}$ [NBT], where $k_{NBT}$ (pH = 7.8) = $5.94 \times 10^4$ $M^{-1} s^{-1}$.[45,46] Hence, the catalytic rate constant, $k_{cat}$ = $k_{NBT}$ [NBT]/$IC_{50}$, was calculated to be $k_{cat}$ = $1.91 \times 10^6$ $M^{-1} s^{-1}$. This value is independent of the detector concentration and appropriate for comparison with literature values. The SOD-like activity of the Mn-salbutO complex is similar to that of Mn-salen [$k_{cat} = 8 \times 10^5$, $H_2$salen = 1,2-bis(salicylidenamino)ethane],[6] and higher than those of other Mn-SOD mimics with open chain ligands having phenolato,[47] pyridyl,[48] benzymidazolyl,[17] and pyrazolyl[49] donor sites. These results clearly indicate that [Mn(salbutO)] is a suitable SOD mimic.

It has been observed that the catalytic rate constants for the dismutation of the superoxide anion are related to the metal-centered reduction potential of $Mn^{III}$ compounds.[50] The closer this potential approaches the midpoint potential between the oxidation and reduction of $O_2^{\cdot-}$ ($E_{1/2}$ = 0.12 V vs. Ag/AgCl) the more potent the mimic. The $Mn^{III}/Mn^{II}$ potential of [Mn(salbutO)] is too negative to account for any efficient redox cycling of $O_2^{\cdot-}$. Thus, it is the accessibility of the $Mn^{IV}$ state that enables this complex to redox cycle $O_2^{\cdot-}$ and be a powerful SOD mimic.

### *CAT Activity*

The catalytic activity of complexes **1** and **2** toward $H_2O_2$ disproportionation was investigated in methanol and dmf at 25 °C. Addition of $H_2O_2$ to previously stabilized dmf or methanol solutions of complexes **1** and **2** causes immediate vigorous evolution of dioxygen. Volumetric measurements of evolved $O_2$ showed that, in dmf, these complexes are able to disproportionate more than 1200 equiv. of $H_2O_2$ with only slight lowering of activity. During catalytic disproportionation of $H_2O_2$, the LMCT band shifts to lower wavelengths, and a new electronic transition is observed at 510 nm [Figure 9 (a)]. This band, which appears at very short reaction times and disappears when $O_2$ evolution has ceased, may account for the formation of a catalyst–substrate adduct, generated by direct binding of $H_2O_2$ to the complex through ligand-shift. Formation of this intermediate is consistent with the increase in intensity of the 510 nm band with increasing [$H_2O_2$] or [catalyst]. The absence of a signal in the EPR spectra taken during the reaction excludes the possibility that this intermediate corresponds to a mixed-valence or $Mn^{II}$ species. At the end of the reaction, the electronic spectrum and the cyclic voltammogram [inset in Figure 9 (a)] of the final form of the catalyst are analogous to those of the starting dmf solutions of the complex. In methanol, these complexes are able to disproportionate up to 200 equiv. of $H_2O_2$, and then they are inactivated. In this solvent, the absorption pattern of the electronic spectra shows only slight changes during the reaction course [Fig-

 © 2010 Wiley-VCH Verlag GmbH & Co. KGaA, Weinheim 

ure 9 (b)]. In the protic solvent, the monomer/dimer equilibrium shifts toward the monomer, reducing the concentration of dimer available for catalase activity.

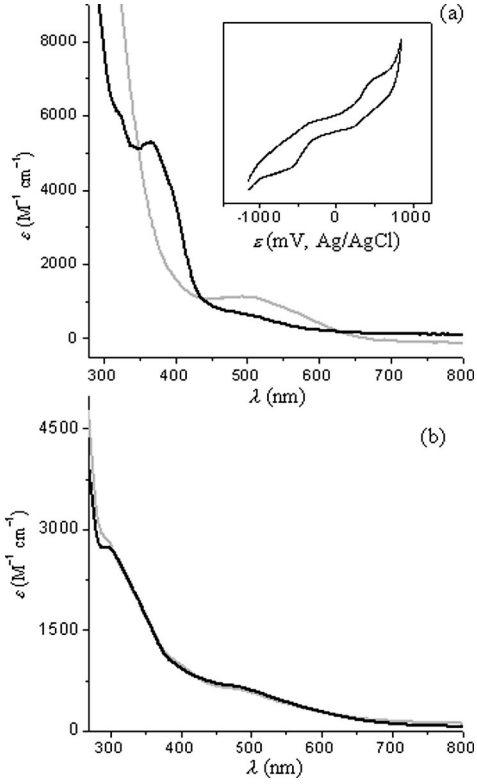


Figure 9. Electronic spectra of **2** before (black line) and after (gray line) addition of 300 equiv. of $H_2O_2$, in (a) dmf (b) methanol. Inset: Cyclic voltammogram at the end of the reaction in dmf.

The initial rate of disproportionation of $H_2O_2$ was determined as a function of the complex and substrate concentrations in methanol and dmf by measuring dissolved oxygen with a Clark-type electrode. It was found that, in both solvents, complexes **1** and **2** afford identical kinetic parameters. In dmf, the reaction is first-order in catalyst and $H_2O_2$ (Figure 10) with a second-order rate constant ($k_{cat}$), obtained from the slope of $r_i$/[cat] ($s^{-1}$) vs. [$H_2O_2$], of $5.6 \pm 0.1$ $M^{-1} s^{-1}$. In methanol, the reaction is second-order in catalyst (Figure S5) and first order in $H_2O_2$, with a third-order $k_{cat}$ of $1.6 \pm 0.2$ $M^{-2} s^{-1}$. The different dependence of the rate of $H_2O_2$ disproportionation on catalyst concentration in the two solvents may be interpreted in terms of the unfavorable effect of the protic solvent on dimer formation. Thus, in methanol, where an equilibrium between monomer and dimer exists (the monomer being the major form in solution, as observed in the ESI mass spectra), the rate is given by $r = k\ K_{dimer}\ [H_2O_2]\ [cat]^2$, where $K_{dimer}$ is the dimerization equilibrium constant and $k$ is the rate constant for the reaction of the dimer with $H_2O_2$. Distinctly, in dmf, the first-order dependence suggests that dimerization is thermodynamically more favored [$K_{dimer(dmf)} >> K_{dimer(methanol)}$]. Therefore, if the catalyst exists in solution as a preformed dimer, $r = k\ [H_2O_2][dimer]$, just as observed. The increasing dimer/monomer ratio observed in the ESI mass spectra with decreasing proton donor ability of the solvent: methanol + acid to methanol ($\alpha_{methanol} = 0.93$) to acetonitrile ($\alpha_{acetonitrile} = 0.19$), supports that in dmf, a nonprotic solvent ($\alpha_{dmf} = 0$), this ratio should be much higher.

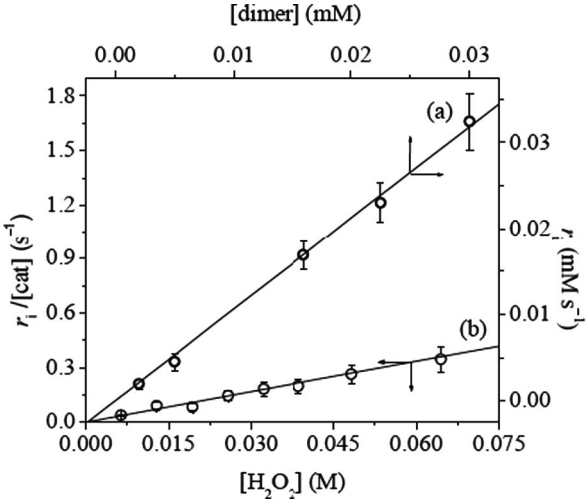


Figure 10. Effect of (a) [catalyst] ($[H_2O_2]_0$ = 12.9 mM) and (b) [$H_2O_2$] on the initial rate of $H_2O_2$ disproportionation at 25 °C in dmf.

The CAT-like activity of the salbutO$^{3-}$ complex, although lower than those observed for other dinuclear or dimeric catalysts, such as $[Mn_2(salpentO)(OMe)(OAc)]^+$ or $[Mn(salpnO)]_2$,[44,51] is significantly higher than those for complexes of the Mn-salen[52] and Mn-bipyridinephenolato[16] series, which also show combined CAT/SOD activities. This result is probably related to the higher proportion of dimer (required for CAT activity) in solutions of the Mn-salbutO complex than in solutions of the Mn-salen and Mn-bipyridinephenolato complexes. Because peroxide is produced in vivo during oxidative stress, the ability to consume $H_2O_2$ is an advantageous property of the Mn-salbutO complex to scavenge reactive oxygen species (ROS).

## Conclusions

The results presented in this work show that $H_3$salbutO is able to stabilize $Mn^{IV}$ under conditions where related symmetric Schiff bases yield $Mn^{III}$ complexes: the shorter $H_3$salpnO affords mononuclear $Mn^{III}$ complexes, their dimers, or polymeric chains;[32,40,53] the longer $H_3$salpentO yields dinuclear $Mn^{III}$ complexes.[44,54–56] Thus, the length and symmetry of the aliphatic bridging units between the central alcohol function and the imino-*N* donor sites of salbutO$^{3-}$ modulates not only the structure of the resulting complex but also the Mn oxidation state.

Complexes [Mn(salbutO)$N_3$] and [Mn(salbutO)SCN] are not stable in methanol or diluted dmf solutions and convert to [$Mn^{III}$(salbutO)] in equilibrium with the dimer. The ligand arrangement around the metal in the monomer is close to that in the dimeric form of the $Mn^{III}$ complex, as no additional resonances are observed in the $^1$H NMR spectra of the complexes. The fact that Mn-salbutO$^{3-}$ shows

 © 2010 Wiley-VCH Verlag GmbH & Co. KGaA, Weinheim 

better SOD and CAT activities than those of catalysts of the Mn-salen series[16] makes this complex particularly attractive as ROS scavenger for pharmaceutical purposes. The ligand arrangement around Mn and the additional alkoxido donor site in the Mn-salbutO$^{3-}$ complex shift the metal-centered redox potentials to values lower than those in Mn-salen. This facilitates the redox reaction through the $Mn^{III}$/$Mn^{IV}$ cycle and results in improved activity.

## Experimental Section

**Materials:** All reagents or AR chemicals were used as purchased. Solvents were purified by standard methods. The concentration of $H_2O_2$ stock solution was determined by iodometric titration.

**1,4-Bis(salicylidenamino)butan-2-ol ($H_3$salbutO):** $H_3$salbutO was prepared by Schiff base condensation of salicylaldehyde with 1,4-diaminobutan-2-ol[57] in ethanol at 60 °C, and was isolated as a pure yellow solid by precipitation from the reaction mixture at room temperature. Yield: 73%. $C_{18}H_{20}N_2O_3$ (312.37): calcd. C 69.21, H 6.45, N 8.97; found C 69.31, H 6.34, N 8.92. $^1$H NMR (200 MHz, [D$_6$]dmso, 25 °C, TMS): $\delta$ = 8.66 (s, 2 H, N=C*H*-), 7.44 (m, 4 H, Ar), 6.99 (m, 4 H, Ar), 3.93–3.80 [m, 5 H, *H*-C(OH)-, -C*H*$_2$-N=C], 1.90 [m, 2 H, (OH)CH-C*H*$_2$-CH$_2$] ppm. Significant IR bands (KBr): $\tilde{\nu}$ = 3425 (OH, broad), 3048, 2921, 2850 (CH), 1634 (C=N), 1609 (Ar), 754, 740 (CH rock) cm$^{-1}$.

**[Mn(salbutO)(N$_3$)]·0.5H$_2$O (1·0.5H$_2$O):** To a solution of freshly prepared Mn(OAc)$_3$·2H$_2$O (86 mg, 0.32 mmol) and $H_3$salbutO (0.1 g, 0.32 mmol) in methanol (8 mL) was added $NaN_3$ (42 mg, 0.64 mmol) in methanol (2 mL), and the reaction mixture was stirred for 24 h. A dark brown microcrystalline precipitate formed, which was collected by filtration, washed with methanol, and dried under vacuum. Yield: 75 mg (0.18 mmol, 58%). $C_{18}H_{17}MnN_5O_3$·0.5H$_2$O (415.30): calcd. C 52.06, H 4.37, Mn 13.2, N 16.86; found C 51.91, H 4.19, Mn 13.4, N 16.53. Significant IR bands (KBr): $\tilde{\nu}$ = 3452 (OH, broad), 3052, 3019, 2940, 2914, 2875 (CH), 2032 (N$_3$), 1617 (C=N), 1596 (Ar), 757 (CH rock), 613, 576, 449, 410 (MnL) cm$^{-1}$. Molar conductivity = 69 $\Omega^{-1}$cm$^2$M$^{-1}$. Single crystals of **1** suitable for X-ray diffraction were obtained from the filtrate of the reaction mixture, which was left to stand for several days.

**[Mn(salbutO)(SCN)]·2H$_2$O (2·2H$_2$O):** To a solution of Mn(OAc)$_3$·2H$_2$O (172 mg, 0.64 mmol) and $H_3$salbutO (0.10 g, 0.32 mmol) in methanol (5 mL) was added KSCN (195 mg, 2.1 mmol) in water (1 mL), and the reaction mixture was stirred for 24 h. A dark brown microcrystalline precipitate formed, which was collected by filtration, washed with methanol, and dried under vacuum. Yield: 0.14 g (0.3 mmol, 94%). $C_{19}H_{17}MnN_3O_3S$·2H$_2$O (458.39): calcd. C 49.78, H 4.58, Mn 12.0, N 9.17, S 6.99; found C 49.86, H 3.74, Mn 13, N 9.01, S 6.98. Significant IR bands (KBr): $\tilde{\nu}$ = 3413 (OH, broad), 3049, 3025, 2921, 2865 (CH), 2058 (SCN), 1618 (C=N), 1598 (Ar), 757 (CH rock), 613, 577, 455 (MnL) cm$^{-1}$. Molar conductivity = 64 $\Omega^{-1}$ cm$^2$ M$^{-1}$.

**Physical Measurements:** Electronic spectra were recorded with a JASCO V550 spectrophotometer having thermostatted cell compartments. IR spectra were recorded with a Perkin–Elmer Spectrum One FTIR spectrophotometer. Electrospray ionization (ESI) mass spectra were recorded with a Perkin–Elmer SCIEX 365 LCMSMS mass spectrometer, by using ca. $10^{-5}$ M solutions of the complexes in methanol at a flow rate of 5 μL min$^{-1}$. EPR measurements were made with a Bruker ESP 300 E spectrometer by using a microwave frequency generated by a Bruker ER 04 (9–10 GHz) instrument. $^1$H NMR spectra were recorded with a Bruker AC 200 NMR spectrometer at ambient probe temperature (ca. 26 °C), with a nominal operating frequency of 200.1 MHz. Variable-temperature magnetic susceptibility data were obtained with a Quantum Design MPMS SQUID susceptometer, under a magnetic field of 1.0 T (**1**) and 0.5 T (**2**) in the temperature range 2–300 K. Diamagnetic corrections were applied by using Pascal's constants.[58] Least-squares fittings were accomplished with an adapted version of the function-minimization program *MINUIT*.[59] Conductivity measurements were performed by using a Horiba F-54 BW conductivity meter, on 1.0 mM solutions of the complexes in methanol. The electrochemical experiments were performed with a computer-controlled Princeton Applied Research potentiostat, model VERSASTAT II, with model 270/250 Research Electrochemistry Software. Studies were carried out under Ar, in dmf or methanol solutions with $Bu_4NPF_6$ (0.1 M) as supporting electrolyte and a ca. $10^{-3}$ M solution of the complex. The working electrode was a Pt wire and the reference electrode was Ag/AgCl with Pt as the auxiliary electrode. Using the described conditions, the ferrocene/ferrocenium redox couple was observed at $E_{1/2}$ = 417 mV in methanol and $E_{1/2}$ = 491 mV in dmf.

**Disproportionation of H$_2$O$_2$:** The stoichiometry of the $H_2O_2$ disproportionation catalyzed by **1** and **2** was measured by volumetric determination of $O_2$ evolved from reaction mixtures in dmf or methanol as described previously.[60] Kinetic studies were carried out polarographically by using a Clark-type oxygen electrode with an YSI oxygen-monitoring system (Model 5300, Yellow Springs Instruments Co., Inc.). The initial rate method was used to determine the rate constants (see ref.[60] for further details). Each rate constant reported here represents the average value of multiple determinations that fall within ±5%.

**Indirect SOD Assay:** The SOD activity of the complexes was assayed by measuring inhibition of the photoreduction of nitro blue tetrazolium (NBT), by a slightly modified version of the method originally described by Beauchamps and Fridovich.[61] The solutions containing riboflavin ($3.4 \times 10^{-6}$ M), methionine (0.01 M), NBT ($4.6 \times 10^{-5}$ M), and complex of various concentrations were prepared with phosphate buffer (pH 7.8). The mixtures were illuminated with a fluorescent lamp with constant light intensity at 25 °C. The reduction of NBT was monitored at 560 nm with various illumination periods ($t$). Rates in the absence and in the presence of complex were determined for each concentration of complex added and plotted against it. Inhibition percentage was calculated according to: $\{(\Delta Abs/t)_{without\ complex} - (\Delta Abs/t)_{with\ complex}\} \times 100/(\Delta Abs/t)_{without\ complex}$. The $IC_{50}$ value represents the concentration of the SOD mimic that induces a 50% inhibition of the reduction of NBT. Control experiments were performed on mixtures of NBT + complex, riboflavin + complex, and NBT + methionine + complex, in phosphate buffer, to ensure that the complex does not react independently with any of the components of the mixture. On the basis of these experiments, cross reactivity of the complex with NBT or riboflavin was disregarded. Under conditions used in this work, the catalytic rate constant ($k_{McCF}$) for MnSOD was found to be $5.5 \times 10^8$ M$^{-1}$ s$^{-1}$, a value consistent with that reported in the literature.[62]

**X-ray Crystal Structure Determination:** Crystallographic data for compound **1**, [Mn(salbutO)(N$_3$)], were collected at 180 K with an Oxford-Diffraction XCALIBUR CCD Diffractometer equipped with a Cryojet cooler device from Oxford Instruments and a graphite-monochromated Mo-$K_\alpha$ radiation source. The unit cell determination and data integration were carried out by using the *CrysAlis*

 © 2010 Wiley-VCH Verlag GmbH & Co. KGaA, Weinheim 

package.[63] The structure was solved with *SIR 92*[64] and refined by full-matrix least-squares on $F_o$ with *CRYSTALS*,[65] with anisotropic displacement parameters for non-hydrogen atoms. The H atoms were all located in a difference map, but those attached to carbon atoms were repositioned geometrically. The H atoms were initially refined with soft restraints on the bond lengths and angles to regularize their geometry and isotropic displacement parameters in the range 1.2–1.5 times $U_{eq}$ of the parent atom, after which the positions were refined with riding constraints. Absorption corrections were applied by using *Multiscan*.[66] The molecular plots were drawn with *Cameron*[67] and *Mercury*.[68] Crystal data collection and refinement parameters for **1** at 180 K: Mo-$K_\alpha$ ($\lambda$ = 0.71073 Å), $C_{18}H_{17}MnN_5O_3$, $M_r$ = 406.297, dark brown needles, dimensions 0.1 × 0.1 × 0.25 mm, monoclinic, space group: $P12_1/n1$, $a$ = 8.0780(5) Å, $b$ = 12.2813(10) Å, $c$ = 17.2752(12) Å, $\beta$ =97.074(6)°, $V$ = 1700.8(2) Å$^3$, $Z$ = 4, $\rho_{cald}$ = 1.59 Mg m$^{-3}$, $\mu_{mo}$ = 0.807 mm$^{-1}$, $F(000)$ = 836.000, $\theta$ range: 3 to 29°, 15798 reflections measured, 4543 unique, 244 refined parameters, GOOF for $F^2$ 1.0871, $wR([\Sigma w(|F_o^2| - |F_c^2|)^2/\Sigma\ w|F_o^2|^2]^{1/2})$ = 0.040, $R(\Sigma||F_o| - |F_c||/\Sigma|F_o|)$ = 0.034.

CCDC-743344 contains the supplementary crystallographic data for this paper. These data can be obtained from The Cambridge Crystallographic Data Centre free of charge via www.ccdc.cam.ac.uk/data_request/cif.

**Supporting Information** (see footnote on the first page of this article): Hydrogen-bonding interactions and magnetism for complex **1**, effect of catalyst on $H_2O_2$ disproportionation in methanol, simulated mass spectra, and ESI mass spectra of **2** in methanol and $HClO_4$/methanol.

## Acknowledgments

We thank the National University of Rosario, the Consejo Nacional de Investigaciones Científicas y Técnicas (CONICET), and the National Agency for Sciences Promotion for financial support, and CONICET and Centre National de la Recherche Scientifique (CNRS) for a bilateral agreement (Res.709/2005).

[1] V. L. Pecoraro (Ed.), *Manganese Redox Enzymes*, VCH, New York, **1992**.
[2] W. C. Stallings, K. A. Pattridge, R. A. Strong, M. L. Ludwig, *J. Biol. Chem.* **1985**, *260*, 16424–16432.
[3] M. W. Parker, C. C. Blake, *J. Mol. Biol.* **1988**, *199*, 649–661.
[4] S. V. Antonyuk, V. V. Barynin, *Crystallogr. Rep.* **2000**, *45*, 105–116.
[5] V. V. Barynin, M. M. Whittaker, S. V. Antonyuk, V. S. Lamzin, P. M. Harrison, P. J. Artymiuk, J. W. Whittaker, *Structure* **2001**, *9*, 725–738.
[6] D. P. Riley, *Chem. Rev.* **1999**, *99*, 2573–2588.
[7] D. Salvemini, Z. Wang, J. Zweier, A. Samouilov, H. Macarthur, T. Mismo, M. Currie, S. Cuzzocrea, J. Sikorski, D. Riley, *Science* **1999**, *286*, 304–306.
[8] G. F. Liu, M. Filipovic, F. W. Heinemann, I. Ivanovic-Burmazovic, *Inorg. Chem.* **2007**, *46*, 8825–8835.
[9] A. Maroz, G. F. Kelso, R. A. J. Smith, D. C. Ware, R. F. Anderson, *J. Phys. Chem. A* **2008**, *112*, 4929–4935.
[10] A. J. Wu, J. E. Penner-Hahn, V. L. Pecoraro, *Chem. Rev.* **2004**, *104*, 903–938.
[11] S. Signorella, A. Rompel, K. Buldt-Karentzopoulos, B. Krebs, V. L. Pecoraro, J.-P. Tuchagues, *Inorg. Chem.* **2007**, *46*, 10864–10868.
[12] J. W. De Boer, W. R. Browne, B. L. Feringa, R. Hage, *C. R. Chim.* **2007**, *10*, 341–354.
[13] S. Signorella, J.-P. Tuchagues, D. Moreno, C. Palopoli in *Inorganic Biochemistry Research Progress* (Eds.: J. G. Hughes, A. J. Robinson), Nova Science Publishers, Inc., New York, **2008**, pp. 243–279.
[14] B. K. Shin, Y. Kim, M. Kim, J. Han, *Polyhedron* **2007**, *26*, 4557–4566.
[15] L. Dubois, J. Pécaut, M. F. Charlot, C. Baffert, M. N. Collomb, A. Deronzier, J. M. Latour, *Chem. Eur. J.* **2008**, *14*, 3013–3025.
[16] G. M. P. Giblin, P. C. Box, I. B. Campbell, A. P. Hancock, S. Roomans, G. I. Mills, C. Molloy, G. E. Tranter, A. L. Walker, S. R. Doctrow, K. Huffman, B. Malfroy, *Bioorg. Med. Chem. Lett.* **2001**, *11*, 1367–1370.
[17] Q. X. Li, Q. H. Luo, Y. Z. Li, Z. Q. Pan, M. C. Shen, *Eur. J. Inorg. Chem.* **2004**, 4447–4456.
[18] K. Baker, C. Bucay Marcus, K. Huffman, H. Kruk, B. Malfroy, S. R. Doctrow, *J. Pharmacol. Exp. Ther.* **1998**, *284*, 215–221.
[19] H. Chun, P. Chaudhuri, T. Weyhermller, K. Weighardt, *Inorg. Chem.* **2002**, *41*,790–795.
[20] M. Yuan, F. Zhao, W. Zhang, Z. M. Wang, S. Gao, *Inorg. Chem.* **2007**, *46*, 11235–11242.
[21] K. R. Reddy, M. V. Rajasekharan, J.-P. Tuchagues, *Inorg. Chem.* **1998**, *37*, 5978–5982.
[22] S. K. Chandra, A. Chakravorty, *Inorg. Chem.* **1992**, *31*, 760–765.
[23] S. K. Chandra, P. Basu, D. Ray, S. Pal, A. Chakravorty, *Inorg. Chem.* **1990**, *29*, 2423–2428.
[24] S. Duta, P. Basu, A. Chakravorty, *Inorg. Chem.* **1991**, *30*, 4031–4037.
[25] P. S. Pavacik, J. C. Huffman, G. Christou, *J. Chem. Soc., Chem. Commun.* **1986**, 43–44.
[26] D. P. Kessissoglou, X. Li, W. M. Butler, V. L. Pecoraro, *Inorg. Chem.* **1987**, *26*, 2487–2492.
[27] S. M. Saadeh, M. S. Lah, V. L. Pecoraro, *Inorg. Chem.* **1991**, *30*, 8–15.
[28] M. Mikuriya, D. Jie, Y. Kakuta, T. Tokii, *Bull. Chem. Soc. Jpn.* **1993**, *66*, 1132–1139.
[29] T. M. Rajendiran, J. W. Kampf, V. L. Pecoraro, *Inorg. Chim. Acta* **2002**, *339*, 497–502.
[30] a) B. Mabad, J.-P. Tuchagues, P. Cassoux, D. N. Hendrickson, *Inorg. Chem.* **1986**, *25*, 1420–1431; b) D. P. Kessissoglou, W. M. Butler, V. L. Pecoraro, *Inorg. Chem.* **1987**, *26*, 495–503; c) D. Luneau, J. M. Savariault, J.-P. Tuchagues, *Inorg. Chem.* **1988**, *27*, 3912–3918; d) L. Stelzig, B. Donnadieu, J.-P. Tuchagues, *Angew. Chem. Int. Ed. Engl.* **1997**, *36*, 2221–2222; e) L. Stelzig, A. Steiner, B. Chansou, J.-P. Tuchagues, *Chem. Commun.* **1998**, 771–772.
[31] a) V. L. Pecoraro, W. M. Butler, *Acta Crystallogr., Sect. C* **1986**, *42*, 1151–1154; b) E. J. Larson, V. L. Pecoraro, *J. Am. Chem. Soc.* **1991**, *113*, 3810–3818.
[32] K. Bertoncello, G. D. Fallon, K. S. Murray, E. R. T. Tiekink, *Inorg. Chem.* **1991**, *30*, 3562–3568.
[33] J. W. Gohdes, W. H. Armstrong, *Inorg. Chem.* **1992**, *31*, 368–373.
[34] a) Z. Zhang, C. Brouca-Cabarrecq, C. Hemmert, F. Dahan, J.-P. Tuchagues, *J. Chem. Soc., Dalton Trans.* **1995**, 1453–1460; b) X. Xia, M. Verelst, J.-C. Daran, J.-P. Tuchagues, *J. Chem. Soc., Chem. Commun.* **1995**, 2155–2157; c) N. Matsumoto, Y. Sunatsuki, H. Miyasaka, Y. Hashimoto, D. Luneau, J.-P. Tuchagues, *Angew. Chem. Int. Ed.* **1999**, *38*, 171–173; d) J.-P. Costes, F. Dahan, B. Donnadieu, M.-J. Rodriguez Douton, A. Bousseksou, J.-P. Tuchagues, *Inorg. Chem.* **2004**, *43*, 2736–2744; e) S. Deoghoria, S. K. Bera, B. Moulton, M. J. Zaworotko, J.-P. Tuchagues, G. Mostafa, T.-H. Lu, S. K. Chandra, *Polyhedron* **2005**, *24*, 343–350; f) G. Bhargavi, M. V. Rajasekharan, J.-P. Costes, J.-P. Tuchagues, *Polyhedron* **2009**, *28*, 1253–1260; g) G. Bhargavi, M. V. Rajasekharan, J.-P. Tuchagues, *Inorg. Chim. Acta* **2009**, *362*, 3247–3252.
[35] M. Maneiro, M. R. Bermejo, A. Sousa, M. Fondo, A. M. González, A. Sousa-Pedrares, C. A. McAuliffe, *Polyhedron* **2000**, *19*, 47–54.

 © 2010 Wiley-VCH Verlag GmbH & Co. KGaA, Weinheim 

[36] a) M. W. Lynch, D. N. Hendrickson, B. J. Fitzgerald, C. G. Pierpont, *J. Am. Chem. Soc.* **1984**, *106*, 2041–2049; b) J. R. Hartmann, B. M. Foxman, S. R. Cooper, *Inorg. Chem.* **1984**, *23*, 1381–1387; c) D. T. Richens, C. G. Smith, D. T. Sawyer, *Inorg. Chem.* **1979**, *18*, 706–712; d) K. Wieghardt, U. Bossek, D. Ventur, J. Weiss, *J. Chem. Soc., Chem. Commun.* **1985**, 347; e) M. J. Camenzind, F. J. Hollander, C. L. Hill, *Inorg. Chem.* **1982**, *21*, 4301–4308.
[37] K. Konig, V. P. Desai, B. Kanellakopulos, R. Klenze, *Chem. Phys.* **1980**, *54*, 109–113.
[38] D. Pursche, M. U. Triller, C. Slinn, N. Reddig, A. Rompel, B. Krebs, *Inorg. Chim. Acta* **2004**, *357*, 1695–1702.
[39] M. Hoohenraad, K. K. Ramkisoensing, W. L. Driessen, H. Kooijman, A. L. Spek, E. Bowman, J. G. Haasnoot, J. Reedijk, *Inorg. Chim. Acta* **2001**, *320*, 117–126.
[40] J. Bonadies, M. Maroney, V. L. Pecoraro, *Inorg. Chem.* **1989**, *28*, 2044–2051.
[41] M. T. Caudle, P. Riggs-Gelasco, A. K. Gelasco, J. E. Penner-Hahn, V. L. Pecoraro, *Inorg. Chem.* **1996**, *35*, 3577–3584.
[42] M. R. Bermejo, A. M. González, M. Fondo, A. García-Deibe, M. Maneiro, J. Sanmartín, O. Hoyos, M. Watkinson, *New J. Chem.* **2000**, *24*, 235–241.
[43] M. R. Bermejo, A. M. González-Noya, V. Abad, M. I. Fernández, M. Maneiro, R. Pedrido, M. Vásquez, *Eur. J. Inorg. Chem.* **2004**, 3696–3705.
[44] V. Daier, H. Biava, C. Palopoli, S. Shova, J.-P. Tuchagues, S. Signorella, *J. Inorg. Biochem.* **2004**, *98*, 1806–1817.
[45] S. Durot, C. Policar, F. Cisnetti, F. Lambert, J.-P. Renault, G. Pelosi, G. Blain, H. Korri-Youssoufi, J.-P. Mahy, *Eur. J. Inorg. Chem.* **2005**, 3513–3523.
[46] Z. R. Liao, X. F. Zheng, B. S. Luo, L. R. Shen, D. F. Li, H. L. Liu, W. Zhao, *Polyhedron* **2001**, *20*, 2813–2821.
[47] E. A. Lewis, H. H. Khodr, R. C. Hilder, J. R. Smith, P. H. Walton, *Dalton Trans.* **2004**, 187–188.
[48] J. Lin, C. Tu, H. Lin, P. Jiang, J. Ding, Z. Guo, *Inorg. Chem. Commun.* **2003**, *6*, 262–265.
[49] U. P. Singh, A. K. Sharma, P. Tyagi, S. Upreti, R. K. Singh, *Polyhedron* **2006**, *25*, 3628–3638.
[50] I. Batinic-Haberle, I. Spasojevic, P. Hambright, L. Benov, A. Crumbliss, I. Fridovich, *Inorg. Chem.* **1999**, *38*, 4011–4022.
[51] A. Gelasco, S. Bensiek, V. L. Pecoraro, *Inorg. Chem.* **1998**, *37*, 3301–3309.
[52] S. R. Doctrow, K. Huffman, C. Bucay Marcus, G. Tocco, E. Malfroy, C. A. Adinolfi, H. Kruk, K. Baker, N. Lazarowych, J. Mascarenhas, B. Malfroy, *J. Med. Chem.* **2002**, *45*, 4549–4558.
[53] J. A. Bonadies, M. L. Kirk, M. S. Lah, D. P. Kessissoglou, W. E. Hatfield, V. L. Pecoraro, *Inorg. Chem.* **1989**, *28*, 2037–2044.
[54] H. Biava, C. Palopoli, S. Shova, M. De Gaudio, V. Daier, M. González-Sierra, J.-P. Tuchagues, S. Signorella, *J. Inorg. Biochem.* **2006**, *100*, 1660–1671.
[55] D. Moreno, C. Palopoli, V. Daier, S. Shova, L. Vendier, M. González Sierra, J.-P. Tuchagues, S. Signorella, *Dalton Trans.* **2006**, 5156–5166.
[56] C. Palopoli, M. González-Sierra, G. Robles, F. Dahan, J.-P. Tuchagues, S. Signorella, *J. Chem. Soc., Dalton Trans.* **2002**, 3813–3819.
[57] L. Murase, S. Ueno, S. Kida, *Inorg. Chim. Acta* **1984**, *87*, 155–157.
[58] P. Pascal, *Ann. Chim. Phys.* **1910**, *19*, 5–70.
[59] F. James, M. Roos, "*MINUIT Program, a System for Function Minimization and Analysis of the Parameters Errors and Correlations*"; *Comput. Phys. Commun.* **1975**, *10*, 343–367.
[60] C. Palopoli, B. Chansou, J.-P. Tuchagues, S. Signorella, *Inorg. Chem.* **2000**, *39*, 1458–1462.
[61] C. Beauchamps, I. Fridovich, *Anal. Biochem.* **1971**, *44*, 276–287.
[62] G. F. Liu, M. Filipovic, F. W. Heinemann, I. Ivanovic-Burmazovic, *Inorg. Chem.* **2007**, *46*, 8825–8835.
[63] *CrysAlis RED*, version 1.171, Oxford Diffraction Ltd., Oxford, U. K., **2006**.
[64] A. Altomare, G. Cascarano, C. Giaccovazzo, A. Guagliardi, M. C. Burla, G. Polidori, M. Camalli, *J. Appl. Crystallogr.* **1994**, *27*, 435.
[65] P. W. Betteridge, J. R. Carruthers, R. I. Cooper, K. Prout, D. J. Watkin, *J. Appl. Crystallogr.* **2003**, *36*,1487.
[66] R. H. Blessing, *Acta Crystallogr., Sect. A* **1995**, *51*, 33.
[67] D. J. Watkin, C. K. Prout, L. J. Pearce, *CAMERON*, Chemical Crystallography Laboratory, University of Oxford, Oxford, UK, **1996**.
[68] C. F. Macrae, I. J. Bruno, J. A. Chisholm, P. R. Edgington, P. McCabe, E. Pidcock, L. Rodriguez-Monge, R. Taylor, J. van de Streek, P. A. Wood, *J. Appl. Crystallogr.* **2008**, *41*, 466–470.

Received: October 21, 2009
Published Online: January 12, 2010

 © 2010 Wiley-VCH Verlag GmbH & Co. KGaA, Weinheim 